

SpikeDerain: Unveiling Clear Videos from Rainy Sequences Using Color Spike Streams

Hanwen Liang^{1,#} Xian Zhong^{1,*} Wenxuan Liu^{2,1,#} Yajing Zheng² Wenxin Huang³

Zhaofei Yu² Tiejun Huang²

¹ Wuhan University of Technology ² Peking University ³ Hubei University

{lianghanwen, zhongx}@whut.edu.cn, {liuwx666, yj.zheng}@pku.edu.cn, wenxinhuang_wh@163.com, {yuzf12, tjhuang}@pku.edu.cn

Abstract

Restoring clear frames from rainy videos presents a significant challenge due to the rapid motion of rain streaks. Traditional frame-based visual sensors, which capture scene content synchronously, struggle to capture the fast-moving details of rain accurately. In recent years, neuromorphic sensors have introduced a new paradigm for dynamic scene perception, offering microsecond temporal resolution and high dynamic range. However, existing multimodal methods that fuse event streams with RGB images face difficulties in handling the complex spatiotemporal interference of raindrops in real scenes, primarily due to hardware synchronization errors and computational redundancy. In this paper, we propose a Color Spike Stream Deraining Network (SpikeDerain), capable of reconstructing spike streams of dynamic scenes and accurately removing rain streaks. To address the challenges of data scarcity in real continuous rainfall scenes, we design a physically interpretable rain streak synthesis model that generates parameterized continuous rain patterns based on arbitrary background images. Experimental results demonstrate that the network, trained with this synthetic data, remains highly robust even under extreme rainfall conditions. These findings highlight the effectiveness and robustness of our method across varying rainfall levels and datasets, setting new standards for video deraining tasks. The code will be released soon.

1. Introduction

Rainfall is one of the most common severe weather phenomena, leading to significant degradation in captured videos and images. This degradation not only reduces visual quality, but also significantly impacts the reliability of computer vision tasks that rely on clear input, such as object detection [24] and person re-identification [54]. As shown in

* Corresponding author. # Contributed equally to this work.

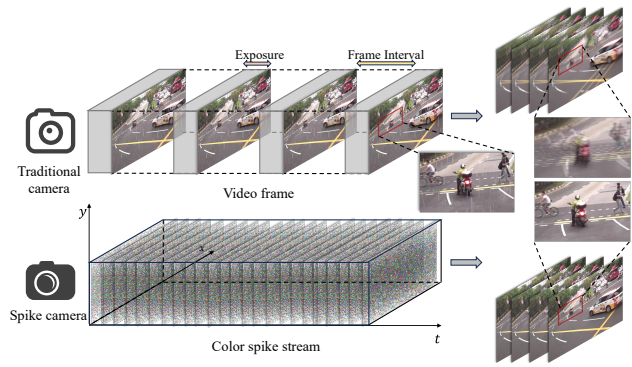


Figure 1. **Comparison of Information Capture between Traditional Video Frames and Spike Streams.** Traditional cameras, due to fixed exposure time and sampling frequency, introduce dynamic blur and inter-frame intervals, which degrade the image quality for subsequent tasks. In contrast, spike streams, with their ultra-high temporal resolution, capture high-speed information more effectively.

Fig. 1, traditional RGB cameras are limited by fixed exposure mechanisms [4], making it difficult to capture the transient motion of high-speed raindrops. This limitation presents a fundamental bottleneck in recovering details in existing frame-based video deraining methods. In recent years, neuromorphic sensors, such as event cameras [15, 31, 34], have provided a new paradigm for dynamic scene perception, offering microsecond temporal resolution and high dynamic range. However, two major challenges remain when reconstructing rain-free images from the high-frequency, asynchronous data stream of neuromorphic sensors: First, the event stream only records sparse events of brightness changes [6], losing absolute brightness and color information, making it difficult to distinguish between rain streaks and background textures. Second, existing multimodal methods [23] that fuse event streams with RGB images struggle to handle the complex spatiotemporal interference of raindrops

in real scenes due to hardware synchronization errors [28] and computational redundancy.

To address these challenges, we propose the first spike-driven single-modal rain removal framework. Unlike event cameras, spike cameras generate spike streams by continuously capturing the absolute brightness of each pixel [8, 22, 57, 58], and spike cameras with a Color Filter Array (CFA) [10–13] retain certain color information while acquiring spike streams. This natural fusion of spatiotemporal continuity and multispectral information offers dual advantages for rain removal tasks: *Physical consistency*, the single-sensor color spike stream eliminates cross-modal alignment errors in high-speed scenes; and *Information integrity*, where the spike sequence preserves both dynamic details and accurate color distribution, mitigating rain streak-background confusion seen in traditional methods.

In this paper, we design a spike-driven deraining network (SpikeDerain) that maps raw spike streams into a continuous spatiotemporal representation through spike density and color correlation, optimizing both image reconstruction and rain streak separation processes. To complement our single-modal spike-driven framework, we introduce a synthetic dataset that addresses two critical challenges: the lack of dynamic continuous rain streaks and the loss of background consistency inherent in event camera data. Our physically interpretable rain streak synthesis model generates parameterized, continuously evolving rain streaks that are well aligned with the high temporal resolution of spike cameras. Experiments show that the network, trained with this synthetic data, remains highly robust under extreme rainfall conditions.

The contributions can be summarized fourfold:

- We utilize the spatiotemporal joint characterization capability of color spike streams to achieve spike-driven single-modal rain removal for the first time.
- We propose a joint optimization deraining network driven by color spike streams, capable of reconstructing dynamic scenes and accurately removing rain streaks.
- We design a parameterized rain streak generator that quantitatively controls the physical properties of rain streaks.
- We achieve significant improvements compared to state-of-the-art methods, with extensive experiments demonstrating the effectiveness of each module.

2. Motivation

Traditional rain removal methods often rely on frame-based processing [29, 47, 49], while spike stream and event stream, as emerging forms of dynamic perception data, provide new ideas [16, 30, 34]. Event cameras and spike cameras use different technological principles when capturing dynamic scenes, and there are significant differences between the two in terms of information capture methods and performance capabilities.

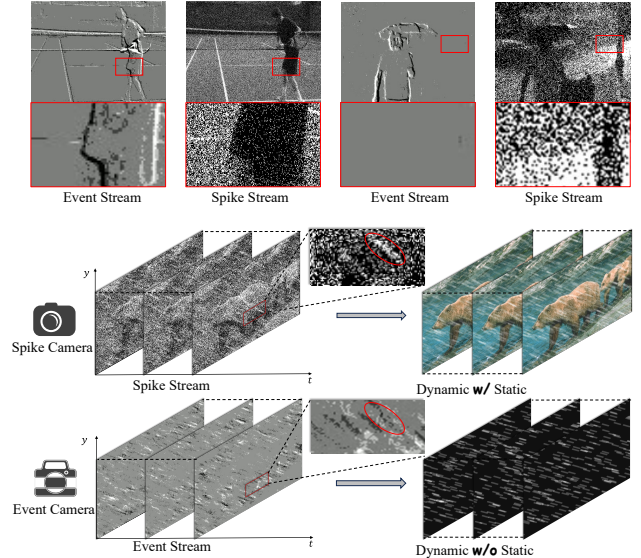


Figure 2. **Difference between Event-based and Our Spike-based Rainy Removal.** Event cameras only record relative light intensity. In contrast, spike cameras record absolute light intensity, thereby preserving essential static information.

Unlike traditional cameras, event cameras have ultra-high temporal resolution and can capture high-speed motion information by responding to relative changes in pixel brightness. However, the event camera only records sparse events of brightness changes [15, 32], and its output lacks absolute brightness and color information of the scene. As shown in Fig. 2, due to the loss of absolute brightness, completely different objects in the event stream data may visually exhibit the same properties, thereby losing more background details. In addition, due to the unique imaging mechanism of event cameras, only changing pixels are recorded in the time stream, resulting in a significant loss of static information when dealing with fixed-angle scenes. To address these issues, existing research typically employs multimodal inputs [23]. However, this leads to complex problems such as data alignment, hardware synchronization [28], and computational redundancy.

In contrast, spike cameras continuously record the absolute brightness information of each pixel [22, 52, 58], generating a spike stream that not only preserves the dynamic details brought by high temporal resolution but also fully preserves the light intensity and color distribution of the scene [11]. This feature makes the spike camera have obvious advantages in video deraining tasks: First, it delivers comprehensive scene information in a single modality, eliminating the need for supplementary sensors; second, its rich absolute brightness data enables precise raindrop-background separation, ensuring superior background reconstruction.

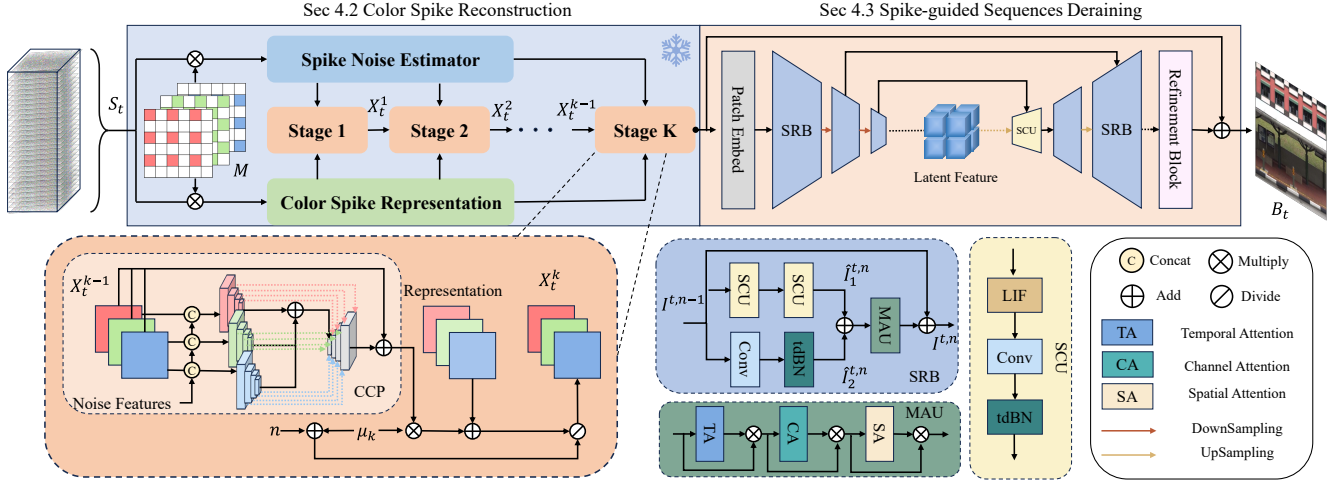


Figure 3. **Architecture of Proposed Spike-Driven Deraining Network (SpikeDerain).** Our method leverages color spike streams from a spike camera by integrating a color spike reconstruction module with a multi-stage SNN-based deraining module to efficiently restore rain-free videos.

3. Related Work

3.1. Video Deraining

Video deraining differs from single-image deraining by exploiting the temporal continuity inherent in video sequences. Early work by Garg and Nayar [17–20] introduced a rain streak removal method based on linear spatiotemporal modeling. Subsequently, researchers improved video deraining performance using various priors, including Fourier domain techniques [1], geometric structures [2], directional features [25], and patch-based methods [40]. Recent advancements in video deraining have been driven by deep learning technologies. For unsupervised training, Yang *et al.* [43] introduced a self-learning method, and Yue *et al.* [46] further improved video deraining by employing semi-supervised learning with a dynamic generator. In this work, we bring in a spike camera, avoiding the challenges of alignment and the computational burden associated with cross-modality.

3.2. Spike-Based Vision

Spike cameras [8, 9, 22, 50] are inspired by the primate retina and differ from traditional cameras by generating synchronized spike streams for each pixel with extremely low latency. Unlike event cameras, spike cameras record absolute light intensity, which enables better recovery of texture details. With their ultra-high temporal resolution and low energy consumption, spike cameras are widely applied in various tasks, including object detection [27, 59], super-resolution [11, 41, 58], dynamic deblurring [6, 48], and motion estimation [53]. These works introduce a spike camera as an innovative sensor that provides complementary information, achieving significant progress. In this paper, we make the first attempt to investigate the role of spike cameras

in video deraining.

3.3. Spiking Neural Networks

SNNs mimic biological neurons by processing information through discrete binary spikes over time, offering energy-efficient computation suited for neuromorphic hardware [3, 35]. While many SNNs [45, 55] are created by converting pre-trained artificial neural networks (ANNs) their performance remains constrained by the original ANN’s architecture. Recent advances in directly training SNNs bypass this limitation [26], achieving competitive accuracy with fewer computational steps. Techniques like surrogate gradients [39] and biologically inspired learning rules enable efficient backpropagation, while architectural innovations (*e.g.*, residual connections adapted for spikes [14]) address vanishing gradients and deepen SNNs effectively. In this work, we propose a directly training SNNs to address video deraining.

4. Proposed Method

We first introduce the working mechanism of the spike camera and the mathematical model of the video deraining task, followed by the reconstruction of the color spike stream and the video deraining module. The overall framework of our method is shown in Fig. 3.

4.1. Preliminaries

Spike Camera Mechanism. The Spike Camera [22] is a neuromorphic sensor that differs fundamentally from traditional RGB and event cameras. In Fig. 4, each photon detector continuously measures the brightness and emits a binary spike once the integrated photon count exceeds a

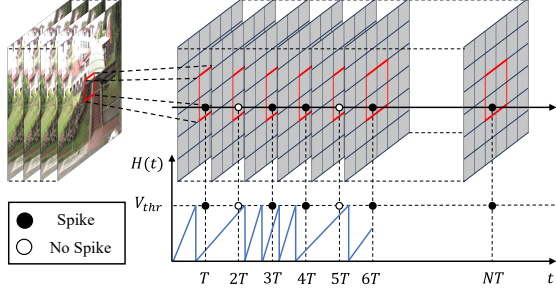


Figure 4. **Spike Camera Mechanism.** Each pixel continuously monitors light intensity and emits a binary spike once a preset brightness threshold is reached, enabling ultra-high temporal resolution capture of dynamic scenes.

preset threshold, after which the integration circuit resets. This generates an asynchronous spike stream $S(x, y, t) \in \{0, 1\}^{H \times W \times 1 \times T}$, where each spike encodes the position (x, y) , timestamp t , and the absolute brightness response of the scene I . The mathematical formulation is as follows:

$$S(x, y, t) = \begin{cases} 1 & \int_{t_0}^t I(x, y, \tau) d\tau \geq \theta, \\ 0 & \text{otherwise,} \end{cases} \quad (1)$$

where $I(x, y, \tau)$ is the instantaneous light intensity, and θ is the spike trigger threshold.

Problem Formulation. Conventional video deraining methods process continuous frames $I = \{I_t\}_{t=1}^n$, where each frame is modeled as the sum of a clean background B_t and a rain streak layer R_t :

$$I_t = B_t + R_t. \quad (2)$$

In contrast, a spike camera produces a spatiotemporal binary spike stream $S \in \{0, 1\}^{H \times W \times 1 \times T}$, where H and W denote the image height and width, and T represents the length of the spike sequence. Spike stream generation can be modeled as follows:

$$S = \mathcal{G}(B + R) + N, \quad (3)$$

where $\mathcal{G}(\cdot)$ is the quantization function of the spike camera, mapping continuous brightness into a binary spike sequence, and N represents the quantization noise, modeled as Poisson-Gaussian noise:

$$N \sim \mathcal{N}(0, \sigma_g^2 + \sigma_p^2 \cdot I_t). \quad (4)$$

To mitigate both rain streak and quantization noise, we propose an optimization objective for joint spike reconstruction and rain removal:

$$\min_{\Phi} \mathcal{L}_{\text{derain}}(G_{\Phi}(F_{\Theta}(S)), B), \quad (5)$$

where $F_{\Theta}(\cdot)$ represents the spike reconstruction module, which maps S to an initial estimation; G_{Φ} is the deraining

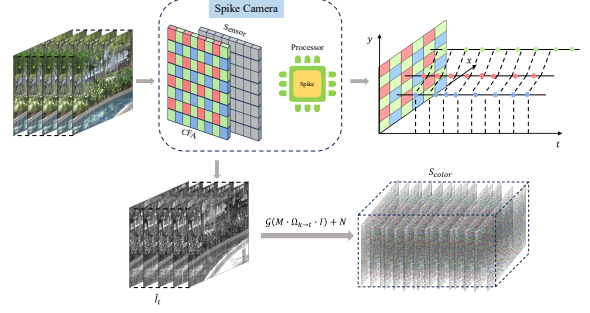


Figure 5. **Color Spike Stream with Bayer CFA.** A color spike stream is obtained using a Bayer pattern, which applies distinct binary masks to capture channel-specific spike signals, thereby enabling robust color reconstruction in dynamic environments.

module, which separates the background from the rain layer. $\mathcal{L}_{\text{recon}}$ and $\mathcal{L}_{\text{derain}}$ represent the reconstruction loss and rain removal loss, respectively.

4.2. Color Spike Reconstruction

Color Spike Stream with Bayer CFA. To capture color information in dynamic scenes, a Bayer-pattern color filter array (CFA) is integrated with the spike camera, enabling the camera to generate distinct spike signals for each color channel at specific pixel locations. It can be defined as:

$$M = M_r + M_g + M_b, \quad (6)$$

where $M_r, M_g,$ and $M_b \in \{0, 1\}^{H \times W}$ are binary masks for the respective color channels, H and W are the image height and width. In high-speed scenes with short exposures, light intensity frames $\{\hat{I}_1, \hat{I}_2, \dots, \hat{I}_n\}$ captured by spike cameras are generated from dynamic scenes using a temporal window. The t -th latent light intensity frame \hat{I}_t is modeled as:

$$\hat{I}_t = M \cdot \Omega_{k \rightarrow t} \cdot I, \quad t \in \{1, 2, \dots, n\}, \quad (7)$$

where I is the target light intensity to be reconstructed from the spike frames, and $\Omega_{k \rightarrow t}$ denotes the motion transformation matrix from the reference frame k to the t -th frame. As shown in Fig. 5, these noisy latent frames are processed by the spike camera mechanism to produce a color spike stream. Thus, Eq. (3) can be modified to:

$$S_{\text{color}} = \mathcal{G}(M \cdot \Omega_{k \rightarrow t} \cdot I) + N. \quad (8)$$

The spike signals generated by each channel are recorded at different positions in S_{color} .

Spike Reconstruction Module. The reconstruction module aims to extract color information and motion patterns from the color spike streams captured by the spike camera. This process involves handling noise in the spike data and predicting missing pixels for each color channel. The module addresses both the temporal and spatial challenges

posed by the Bayer pattern and the binary nature of the spike stream, which includes the **Color Spike Representation (CSR)**, **Spike Noise Estimator (SNE)**, and **Color Correlation Prior (CCP)**.

Initially, the color spike streams are passed through the CSR module, which aligns the temporal features of each color channel, accounting for motion offsets between frames. By multiplying the spike frames with the Bayer mask for each color channel, we obtain frames with missing pixels. A multi-scale 3D convolution encoder processes these frames, extracting temporal features at different scales. These features are fused using an offset-sharing deformable convolution (OSDCN) module, which learns a shared offset for each color channel, aligning features and correcting for motion-induced misalignment across frames. The final output of CSR is a set of aligned feature blocks for each color channel, mathematically formulated as:

$$\text{Output} = \text{Concat}(\text{OSDCN}(\text{3DEncoder}(M_c \cdot S))), \quad (9)$$

where $M_c \cdot S$ represents the separated spike stream by color channel, and $\text{3DEncoder}(\cdot)$ is the multi-scale 3D convolution encoder.

A spike noise estimator (SNE) is employed to estimate noise in spike data, which is affected by mechanical and quantization noise. These noise sources degrade feature extraction quality, making accurate estimation crucial for high-quality detail recovery. The SNE module processes spike frames using a residual block-based encoder to capture noise features for each color channel. A decoder then generates a global noise map, characterizing noise across all channels. Then color correlation prior (CCP) module refines the reconstruction process by capitalizing on spatial and temporal correlation between color channels. Specifically, it concatenates the global noise features N_{global} from SNE with the feature blocks F_r, F_g, F_b obtained from the CSR. This integration facilitates unified processing of color and noise features, enforcing spatiotemporal consistency, and leveraging interchannel dependencies to significantly enhance reconstruction fidelity.

4.3. Spike-guided Sequences Deraining

We propose a novel approach to video deraining by leveraging the SNN framework. This method extends the efficient spiking deraining network [33] to handle continuous video inputs, where temporal dependencies between frames are crucial for accurately removing rain streaks. By processing temporal sequences of frames, our method exploits correlations between consecutive frames, enhancing rain streak removal while preserving important video details.

Spiking Residual Blocks. Given a video input consisting of consecutive frames $I = \{I_1, I_2, \dots, I_n\}$, where n represents the total number of frames, we encode each frame

I_t into spike sequences using a biologically inspired encoding strategy. This converts each pixel’s intensity into a temporal spike stream, representing changes in intensity over time. The Spiking Residual Blocks (SRB) are the core components of our deraining method, processing the temporal spike sequences to capture and remove rain streaks across frames. Each SRB consists of **Spike Convolution Unit (SCU)**, **Mixed Attention Unit (MAU)**, and **Residual Learning**.

The SCU converts the spiking representation into a temporal feature map by simulating membrane potential dynamics. It captures temporal variations and rain patterns by analyzing spike responses across consecutive frames. Leaky integrate-and-fire (LIF) neurons are utilized in the SCU to convert input signals into spike sequences, striking a balance between biological characteristics and computational complexity. The explicit dynamic equations for the LIF neurons can be formulated as:

$$\begin{cases} H^{t,n} = U^{t-1,n} + \frac{1}{\tau} (X^{t,n} - (U^{t-1,n} - V_{\text{reset}})), \\ S^{t,n} = \Theta(H^{t,n} - V_{\text{thr}}), \\ U^{t,n} = (\beta H^{t,n}) \odot (1 - S^{t,n}) + V_{\text{reset}} S^{t,n}, \end{cases} \quad (10)$$

where $H^{t,n}$ is the membrane potential of the neuron at time t and state n , $S^{t,n}$ represents the firing state (1 if the neuron fires a spike, 0 otherwise), and $U^{t,n}$ is the membrane potential update. The neuronal membrane potential $H^{t,n}$ is determined by the membrane potential of the previous time step $U^{t-1,n}$, the input current $X^{t,n}$, and the time constant τ . If the membrane potential exceeds the threshold V_{thr} , the neuron emits a spike, setting $S^{t,n}$ to 1, and the membrane potential resets to V_{reset} . Otherwise, the membrane potential continues to update and decay.

The mixed attention unit (MAU) is designed to improve the efficiency of spike processing by focusing on the most relevant parts of the input spike train. In traditional spike-based models, irrelevant or noisy spike events can distort learned features, reducing the model’s ability to focus on important temporal or spatial components of the signal. The MAU addresses this by applying spatial and temporal attention mechanisms, dynamically adjusting the model’s focus. Spatial attention operates on the spatial dimensions of the input (*e.g.*, spatial locations within an image), while temporal attention selectively focuses on relevant time steps based on the temporal dynamics of the spike events.

Residual learning helps prevent issues such as information loss or gradient vanishing, which can occur in deep networks. By introducing skip connections, it ensures that low-level features are preserved and efficiently propagated across layers. Overall, Assuming that the output of the n -th SRB at the t -th time step is $I^{t,n}$, the calculated process of

SRB can be depicted as:

$$\begin{cases} \hat{I}_1^{t,n} = \text{SCU}(\text{SCU}(I^{t,n-1})), \\ \hat{I}_2^{t,n} = \text{tdBN}(\text{Conv}(I^{t,n-1})), \\ I^{t,n} = \text{MAU}(\hat{I}_1^{t,n} + \hat{I}_2^{t,n}) + I^{t,n-1}, \end{cases} \quad (11)$$

where tdBN refers to threshold-dependent batch normalization (BN), a method designed for SNNs to address the limitations of traditional BN in handling sparse, time-dependent data in spiking neurons.

To align with the characteristics of spike cameras, which capture continuous dynamic information at ultra-high temporal resolution, and to satisfy the spatiotemporal consistency requirements of our video deraining module, we construct a novel dynamic dataset, Rain100C. The rain streaks generated by our method adhere more closely to physical laws in terms of spatial distribution and brightness attenuation, thereby aligning well with the high-frequency data captured by spike cameras.

5. Experimental Results

We present comprehensive experiments conducted on commonly used benchmark datasets to evaluate the effectiveness of the proposed method. The experiments involve rigorous testing and analysis, providing a thorough evaluation of performance.

5.1. Dataset Preparation

RAIN100C Dataset. To obtain image sequences with continuous rain patterns more conveniently, we propose a rain pattern synthesis method based on traditional additive models. By quantitatively adjusting the physical properties of rain patterns (*e.g.*, direction, length, width), we introduce a new paradigm for continuous rain pattern synthesis. Unlike traditional synthetic continuous rain patterns, our proposed model is not limited to similar backgrounds, fixed sizes, or software dependencies. Using our proposed continuous rain pattern synthesis method, we generated RAIN100C, based on RAIN100H [42] background images. For each background image, we generated 14 rain layer with continuous rain streaks, with the physical characteristics of the rain patterns varying across different backgrounds. For more details, please refer to the supplementary materials.

RAINSYNLIGHT25 and RAINSYNHEAVY25 Datasets. These two datasets [49] consist of 190 rainy/sunny video pairs in the training set and 27 pairs in the testing set. The rainy-day sequences were synthesized using probability models. RAINSYNHEAVY25 contains denser rain streaks than RAINSYNLIGHT25, and the corresponding spike signals for both are generated by spike simulators [51].

NTURAIN Dataset. This dataset [5] is divided into two groups: one captured with a slow camera and the other with

a fast camera. It contains 25 pairs of rainfall sequences, including clear training versions and 8 pairs of test versions. For each rain-free video, Adobe After Effects (AE) synthesizes 3 or 4 rain layers with varying settings, which are then added to the video. The color spike stream for this dataset is also generated by a spike simulator [51].

5.2. Implementation Details and Metrics

Implementation Details. During training, we use the Adam optimizer within the PyTorch framework. Initially, the reconstruction module is trained separately, with the CCP modules sharing the same parameters across iterations. The number of input spike frames N is set to 39, and we randomly crop the spike frames into 64×64 patches, with a batch size of 8. Data augmentation is applied by randomly flipping the input frames horizontally and vertically. After completing the reconstruction module training, we freeze the module and train the overall framework using an Adam optimizer with a batch size of 12. The learning rate is set to 1×10^{-3} , and a cosine annealing strategy is used to gradually decrease the learning rate to 1×10^{-7} .

Due to the lack of corresponding spike streams on NTU-RAIN, RAINSYNLIGHT25, and RAINSYNHEAVY25, we used a spike simulator [51] combined with a Bayer Pattern CFA to generate corresponding color spike streams for training our model.

Metrics. We introduce peak signal-to-noise ratio (PSNR) and structural similarity index (SSIM) as quantitative evaluation metrics, computed in the Y channel of the YCbCr color space. To evaluate the efficiency of our method, we also calculate the energy consumption of the model, following the previous works [21].

5.3. Comparisons with State-of-the-Art Methods

We have compared our network with several state-of-the-art methods. Among these, JDNet [37] is single-image deraining methods, MPEVNet [34] and EHNet [16] are event-driven methods, and TransWeather [36] and GridFormer [38] are general models designed to handle various weather conditions.

Quantitative Results on Synthetic Data. Tab. 1 presents the quantitative results of our model compared to other advanced methods on three publicly available datasets and the proposed RAIN100C. Our model outperformed all other methods on all four datasets in terms of both PSNR and SSIM. For example, on NTURAIN, our model achieved a PSNR of 38.14 dB and an SSIM of 0.972, showing a 0.66 dB improvement in PSNR over suboptimal results, ESTIL [49]. On RAINSYNLIGHT25, our model achieved PSNR and SSIM values of 34.48dB and 0.954, second only to ESTIL [49], and far exceeding the latest event-driven models, EHNet [16] and MPEVNet [34]. On RAINSYNHEAVY25,

Method	Venue	NTURAIN		RAINSYNLIGHT25		RAINSYNHEAVY25		RAIN100C	
		PSNR \uparrow	SSIM \uparrow						
SLDNet [44]	CVPR'20	34.26	0.956	28.73	0.843	18.80	0.529	33.42	0.947
D3RNet [29]	CVPR'20	32.53	0.947	28.21	0.879	24.65	0.772	34.22	0.959
JDNet [37]	ACM MM'20	32.95	0.953	28.87	0.886	24.62	0.758	34.61	0.966
S2VD [47]	CVPR'21	37.37	0.968	33.84	0.925	27.77	0.818	<u>38.15</u>	<u>0.972</u>
TransWeather [36]	CVPR'22	33.35	0.955	29.06	0.902	25.95	0.797	36.96	0.969
MPEVNet [34]	CVPR'23	33.49	0.958	30.08	0.904	26.01	0.792	-	-
ESTIL [49]	TPAMI'23	<u>37.48</u>	<u>0.970</u>	36.12	0.963	<u>28.48</u>	<u>0.824</u>	-	-
GridFormer [38]	IJCV'24	32.96	0.954	28.45	0.896	24.66	0.724	36.28	0.963
EHNet [16]	IJCV'24	34.11	0.962	30.63	0.920	26.28	0.811	-	-
SpikeDerain (Ours)		38.14	0.972	<u>34.48</u>	<u>0.954</u>	30.79	0.899	39.24	0.985

Table 1. **Quantitative comparisons on three public datasets and Rain100C.** Best and second-best results are highlighted in **bold** and underlined.

which features a denser distribution of rain streaks, our model achieved PSNR and SSIM values of 30.79 dB and 0.899, respectively, representing an 8% and 9% improvement over suboptimal results, ESTIL [49]. For RAIN100C, which contains a wider variety of rain pattern physical attributes and richer backgrounds, our method also achieved significantly better results compared to other state-of-the-art methods. These results emphasize the effectiveness and robustness of our method across various rainfall levels and datasets, setting new standards for video deraining tasks.

Qualitative Results on Synthetic Data. Fig. 6 presents a qualitative analysis of results on NTURAIN and SYNHEAVY25, which has more complex rain patterns. From the comparison, it is clear that D3RNet [29] and JDNet [37] remove only a small number of rain streaks in high-speed scenes, with many streaks remaining. This aligns with their poor performance in the quantitative results. MPEVNet [34] and EHNet [16] perform better in high-speed scenarios by introducing event streams but still face challenges in different scenarios. S2VD [47] and ESTIL [49] are classic video deraining methods that effectively remove heavy rain streaks but still leave some subtle rain streaks. Among all comparison methods, our approach produces the best results, completing the restoration of detailed textures while extracting high-speed motion features.

5.4. Ablation Studies

To better understand the factors contributing to the superior performance of our method, we conducted ablation studies on RAINSYNHEAVY25.

Effectiveness of Different Time Steps. Tab. 2 shows the performance at various time steps, revealing that longer time windows generally improve image restoration quality by enabling the network to capture richer spatiotemporal features. However, as the time step grows, the computational overhead and energy consumption also increase. Specifically, performance gains begin to plateau beyond five time steps, indicating diminishing returns relative to energy cost.

Time steps	PSNR \uparrow	SSIM \uparrow	FLOPs (G) \downarrow	Energy (uJ) \downarrow
3	30.30	0.895	8.479	1.0565 $\times 10^5$
4	30.58	0.896	8.578	1.0690 $\times 10^5$
5	30.79	0.899	8.678	1.0814 $\times 10^5$
6	30.47	0.894	8.777	1.0939 $\times 10^5$
7	29.72	0.885	8.877	1.1064 $\times 10^5$

Table 2. **Impact of different time steps on RAINSYNHEAVY25.** All time steps are configured during training.

Reconstruction Method	PSNR \uparrow	SSIM \uparrow	LPIPS \downarrow
TFI [56]	28.32	0.843	0.171
TFP [56]	30.34	0.889	0.112
BSN [7]	24.87	0.714	0.477
SpikeDerain (Ours)	30.79	0.899	0.104

Table 3. **Impact of different reconstruction methods on RAINSYNHEAVY25.**

To balance performance and efficiency, we selected a time step of 5 as the default.

Effectiveness of Color Spike Reconstruction. As shown in Fig. 7, the reconstructed pixel intensity histograms closely align with the ground truth in all three channels, indicating that the proposed Color Spike Reconstruction method preserves both the shape of the overall distribution and fine details. This high degree of overlap demonstrates minimal distortion, maintaining spatial continuity and inter-channel consistency without introducing noticeable color shifts or artifacts. Consequently, the reconstructed images effectively retain the original color characteristics, confirming the robustness and accuracy of the method.

Effectiveness of Different Reconstruction Methods. To evaluate the performance of our reconstruction module, we compared it with several common spike reconstruction methods. Tab. 3 shows the PSNR/SSIM/learned perceptual image patch similarity (LPIPS) values of the final rain removal results using different reconstruction methods. To match the color spike stream of the Bayer pattern, we reconstructed the

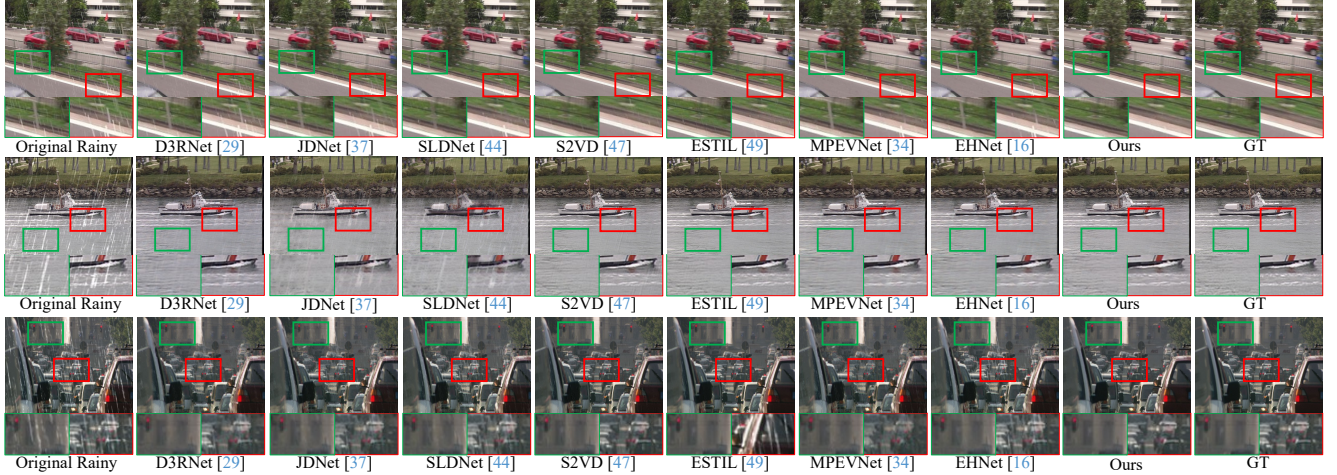


Figure 6. **Qualitative comparison on NTURAIN (Top), SYNHEAVY25 (Middle) and SYNLIGHT25 (Bottom).** The green box highlights thicker rain streaks, while the red box shows more challenging interlaced rain patterns. Zoom-in for better visualization.

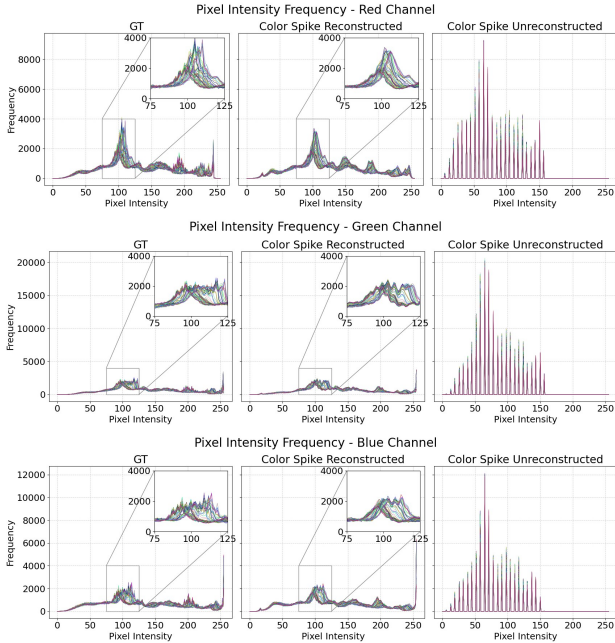


Figure 7. **Pixel Intensity Frequency Analysis.** From top to bottom and from left to right, represent the different pixel frequency analyses of the original image, reconstructed image, and original spike stream in the three channels, respectively.

image into three channels using the CFA mask. The comparison reveals that the traditional TFP method preserves color information less effectively, while the BSN method disrupts color correlation between channels. Our reconstruction method fully preserves color information and avoids color distortion during subsequent processing.

Model	BN	tdBN	CU	SCU	PSNR \uparrow	SSIM \uparrow	LPIPS \downarrow
ANN	●	○	●	○	30.21	0.889	0.126
SNN	●	○	○	●	30.71	0.896	0.112
ANN w/ tdBN	○	●	●	○	29.96	0.876	0.132
SNN w/ tdBN	○	●	○	●	30.79	0.899	0.104

Table 4. **Quantitative ablation study on different components of our network using RAINSYNHEAVY25.** CU replaces the spiking neuron in SCU with an ANN neuron.

Effectiveness of SNN. We further examined the impact of SNNs on deraining performance via a series of ablation studies. As shown in Tab. 4, incorporating spiking neurons and tdBN consistently enhances the overall metrics. Notably, the SCU excels in capturing temporal dynamics and addressing rain streaks. Compared to conventional convolutions, SNN-based operations paired with tdBN yield higher PSNR/SSIM and lower LPIPS, indicating improved visual fidelity. These results underscore the effectiveness of our spiking architecture in exploiting the asynchronous nature of spike data for robust rain removal.

6. Conclusion

In this work, we propose SpikeDerain, a single-modal video deraining framework that leverages color spike streams captured by a novel spike camera. Unlike traditional cameras limited by fixed exposure and motion blur, and event cameras that capture only sparse brightness changes, our spike camera continuously records absolute brightness and color information at ultra-high temporal resolution. This enables our network to effectively reconstruct detailed color images and accurately separate rain streaks from the background, thereby delivering superior deraining performance.

Acknowledge

This work was supported in part by the National Natural Science Foundation of China under Grant 62271361 and 62301213, and the Hubei Provincial Key Research and Development Program under Grant 2024BAB039.

References

- [1] Peter C. Barnum, Srinivasa G. Narasimhan, and Takeo Kanade. Analysis of rain and snow in frequency space. *Int. J. Comput. Vis.*, 86(2-3):256–274, 2010. 3
- [2] Jérémie Bossu, Nicolas Hautière, and Jean-Philippe Tarel. Rain or snow detection in image sequences through use of a histogram of orientation of streaks. *Int. J. Comput. Vis.*, 93(3):348–367, 2011. 3
- [3] Maxence Bouvier, Alexandre Valentian, Thomas Mesquida, François Rummens, Marina Reyboz, Elisa Vianello, and Edith Beigné. Spiking neural networks hardware implementations and challenges: A survey. *ACM J. Emerg. Technol. Comput. Syst.*, 15(2):22:1–22:35, 2019. 3
- [4] Marco Cannici and Davide Scaramuzza. Mitigating motion blur in neural radiance fields with events and frames. In *Proc. IEEE/CVF Conf. Comput. Vis. Pattern Recognit.*, pages 9286–9296, 2024. 1
- [5] Jie Chen, Cheen-Hau Tan, Junhui Hou, Lap-Pui Chau, and He Li. Robust video content alignment and compensation for rain removal in a CNN framework. In *Proc. IEEE/CVF Conf. Comput. Vis. Pattern Recognit.*, pages 6286–6295, 2018. 6
- [6] Kang Chen, Shiyang Chen, Jiyuan Zhang, Baoyue Zhang, Yajing Zheng, Tiejun Huang, and Zhaofei Yu. Spikereveal: Unlocking temporal sequences from real blurry inputs with spike streams. In *Adv. Neural Inf. Process. Syst.*, 2024. 1, 3
- [7] Shiyang Chen, Chaoteng Duan, Zhaofei Yu, Ruiqin Xiong, and Tiejun Huang. Self-supervised mutual learning for dynamic scene reconstruction of spiking camera. In *Proc. Int. Joint Conf. Artif. Intell.*, pages 2859–2866, 2022. 7
- [8] Siwei Dong, Tiejun Huang, and Yonghong Tian. Spike camera and its coding methods. In *Proc. IEEE Data Compress. Conf.*, page 437, 2017. 2, 3
- [9] Siwei Dong, Lin Zhu, Daoyuan Xu, Yonghong Tian, and Tiejun Huang. An efficient coding method for spike camera using inter-spike intervals. In *Proc. IEEE Data Compress. Conf.*, page 568, 2019. 3
- [10] Yanchen Dong, Jing Zhao, Ruiqin Xiong, and Tiejun Huang. 3d residual interpolation for spike camera demosaicing. In *Proc. IEEE Int. Conf. Image Process.*, pages 1461–1465, 2022. 2
- [11] Yanchen Dong, Ruiqin Xiong, Jian Zhang, Zhaofei Yu, Xiaopeng Fan, Shuyuan Zhu, and Tiejun Huang. Super-resolution reconstruction from bayer-pattern spike streams. In *Proc. IEEE/CVF Conf. Comput. Vis. Pattern Recognit.*, pages 24871–24880, 2024. 2, 3
- [12] Yanchen Dong, Ruiqin Xiong, Jing Zhao, Jian Zhang, Xiaopeng Fan, Shuyuan Zhu, and Tiejun Huang. Learning a deep demosaicing network for spike camera with color filter array. *IEEE Trans. Image Process.*, 33:3634–3647, 2024.
- [13] Yanchen Dong, Ruiqin Xiong, Xiaopeng Fan, Shuyuan Zhu, Jin Wang, and Tiejun Huang. Dynamic scene reconstruction for color spike camera via zero-shot learning. *IEEE Trans. Computational Imaging*, 11:129–141, 2025. 2
- [14] Wei Fang, Zhaofei Yu, Yanqi Chen, Tiejun Huang, Timothée Masquelier, and Yonghong Tian. Deep residual learning in spiking neural networks. In *Adv. Neural Inf. Process. Syst.*, pages 21056–21069, 2021. 3
- [15] Xueyang Fu, Chengzhi Cao, Senyan Xu, Fanrui Zhang, Kunyu Wang, and Zheng-Jun Zha. Event-driven heterogeneous network for video deraining. *Int. J. Comput. Vis.*, 132(12):5841–5861, 2024. 1, 2
- [16] Xueyang Fu, Chengzhi Cao, Senyan Xu, Fanrui Zhang, Kunyu Wang, and Zheng-Jun Zha. Event-driven heterogeneous network for video deraining. *Int. J. Comput. Vis.*, 132(12):5841–5861, 2024. 2, 6, 7
- [17] Kshitiz Garg and Shree K. Nayar. Detection and removal of rain from videos. In *Proc. IEEE/CVF Conf. Comput. Vis. Pattern Recognit.*, pages 528–535, 2004. 3
- [18] Kshitiz Garg and Shree K. Nayar. When does a camera see rain? In *Proc. IEEE/CVF Int. Conf. Comput. Vis.*, pages 1067–1074, 2005.
- [19] Kshitiz Garg and Shree K. Nayar. Photorealistic rendering of rain streaks. *ACM Trans. Graph.*, 25(3):996–1002, 2006.
- [20] Kshitiz Garg and Shree K. Nayar. Vision and rain. *Int. J. Comput. Vis.*, 75(1):3–27, 2007. 3
- [21] Yufei Guo, Yuanpei Chen, Xiaode Liu, Weihang Peng, Yuhang Zhang, Xuhui Huang, and Zhe Ma. Ternary spike: Learning ternary spikes for spiking neural networks. In *Proc. AAAI Conf. Artif. Intell.*, pages 12244–12252, 2024. 6
- [22] Tiejun Huang, Yajing Zheng, Zhaofei Yu, Rui Chen, Yuan Li, Ruiqin Xiong, Lei Ma, Junwei Zhao, Siwei Dong, Lin Zhu, Jianing Li, Shanshan Jia, Yihua Fu, Boxin Shi, Si Wu, and Yonghong Tian. 1000x faster camera and machine vision with ordinary devices. *arXiv:2201.09302*, 2022. 2, 3
- [23] Yuya Ichikawa, Ayumu Yamada, Naoko Misawa, Chihiro Matsui, and Ken Takeuchi. Rem-cim: Attentional rgb-event fusion multi-modal analog cim for area/energy-efficient edge object detection during both day and night. *IEICE Trans. Electron.*, 107(10):426–435, 2024. 1, 2
- [24] Ding Jia, Yuhui Yuan, Haodi He, Xiaopei Wu, Haojun Yu, Weihong Lin, Lei Sun, Chao Zhang, and Han Hu. Detsr with hybrid matching. In *Proc. IEEE/CVF Conf. Comput. Vis. Pattern Recognit.*, pages 19702–19712, 2023. 1
- [25] Tai-Xiang Jiang, Ting-Zhu Huang, Xi-Le Zhao, Liang-Jian Deng, and Yao Wang. A novel tensor-based video rain streaks removal approach via utilizing discriminatively intrinsic priors. In *Proc. IEEE/CVF Conf. Comput. Vis. Pattern Recognit.*, pages 2818–2827, 2017. 3
- [26] Jinseok Kim, Kyungsu Kim, and Jae-Joon Kim. Unifying activation- and timing-based learning rules for spiking neural networks. In *Adv. Neural Inf. Process. Syst.*, 2020. 3
- [27] Jianing Li, Xiao Wang, Lin Zhu, Jia Li, Tiejun Huang, and Yonghong Tian. Retinomorphic object detection in asynchronous visual streams. In *Proc. AAAI Conf. Artif. Intell.*, pages 1332–1340, 2022. 3

- [28] Wenxuan Li, Yan Dong, Shaoqiang Qiu, and Bin Han. Hardware-free event cameras temporal synchronization based on event density alignment. In *Proc. Int. Conf. Intell. Robotics Appl.*, pages 60–71, 2023. 2
- [29] Jiaying Liu, Wenhan Yang, Shuai Yang, and Zongming Guo. D3r-net: Dynamic routing residue recurrent network for video rain removal. *IEEE Trans. Image Process.*, 28(2):699–712, 2019. 2, 7
- [30] Zibin Liu, Banglei Guan, Yang Shang, Shunkun Liang, Zhenbao Yu, and Qifeng Yu. Optical flow-guided 6dof object pose tracking with an event camera. In *Proc. ACM Int. Conf. Multimedia*, pages 6501–6509, 2024. 2
- [31] Zibin Liu, Banglei Guan, Yang Shang, Qifeng Yu, and Laurent Kneip. Line-based 6-dof object pose estimation and tracking with an event camera. *IEEE Trans. Image Process.*, 33:4765–4780, 2024. 1
- [32] Zibin Liu, Banglei Guan, Yang Shang, Yifei Bian, Pengju Sun, and Qifeng Yu. Stereo event-based, 6-dof pose tracking for uncooperative spacecraft. *IEEE Trans. Geosci. Remote Sens.*, 63:1–13, 2025. 2
- [33] Tianyu Song, Guiyue Jin, Pengpeng Li, Kui Jiang, Xiang Chen, and Jiyu Jin. Learning a spiking neural network for efficient image deraining. In *Proc. Int. Joint Conf. Artif. Intell.*, pages 1254–1262, 2024. 5
- [34] Shangquan Sun, Wenqi Ren, Jingzhi Li, Kaihao Zhang, Meiyu Liang, and Xiaochun Cao. Event-aware video deraining via multi-patch progressive learning. *IEEE Trans. Image Process.*, 32:3040–3053, 2023. 1, 2, 6, 7
- [35] Amirhossein Tavaneai, Masoud Ghodrati, Saeed Reza Kheradpisheh, Timothée Masquelier, and Anthony Maida. Deep learning in spiking neural networks. *Neural Networks*, 111: 47–63, 2019. 3
- [36] Jeya Maria Jose Valanarasu, Rajeev Yasarla, and Vishal M. Patel. Transweather: Transformer-based restoration of images degraded by adverse weather conditions. In *Proc. IEEE Conf. Comput. Vis. Pattern Recognit.*, pages 2343–2353, 2022. 6, 7
- [37] Cong Wang, Yutong Wu, Zhixun Su, and Junyang Chen. Joint self-attention and scale-aggregation for self-calibrated deraining network. In *Proc. ACM Int. Conf. Multimedia*, pages 2517–2525, 2020. 6, 7
- [38] Tao Wang, Kaihao Zhang, Ziqian Shao, Wenhan Luo, Björn Stenger, Tong Lu, Tae-Kyun Kim, Wei Liu, and Hongdong Li. Gridformer: Residual dense transformer with grid structure for image restoration in adverse weather conditions. *Int. J. Comput. Vis.*, 132(10):4541–4563, 2024. 6, 7
- [39] Ziqing Wang, Yuetong Fang, Jiahang Cao, Qiang Zhang, Zhongrui Wang, and Renjing Xu. Masked spiking transformer. In *Proc. IEEE/CVF Int. Conf. Comput. Vis.*, pages 1761–1771, 2023. 3
- [40] Wei Wei, Lixuan Yi, Qi Xie, Qian Zhao, Deyu Meng, and Zongben Xu. Should we encode rain streaks in video as deterministic or stochastic? In *Proc. IEEE/CVF Int. Conf. Comput. Vis.*, pages 2535–2544, 2017. 3
- [41] Xijie Xiang, Lin Zhu, Jianing Li, Yixuan Wang, TieJun Huang, and Yonghong Tian. Learning super-resolution reconstruction for high temporal resolution spike stream. *IEEE Trans. Circuits Syst. Video Technol.*, 33(1):16–29, 2023. 3
- [42] Wenhan Yang, Robby T. Tan, Jiashi Feng, Zongming Guo, Shuicheng Yan, and Jiaying Liu. Joint rain detection and removal from a single image with contextualized deep networks. *IEEE Trans. Pattern Anal. Mach. Intell.*, 42(6):1377–1393, 2020. 6
- [43] Wenhan Yang, Robby T. Tan, Shiqi Wang, and Jiaying Liu. Self-learning video rain streak removal: When cyclic consistency meets temporal correspondence. In *Proc. IEEE/CVF Conf. Comput. Vis. Pattern Recognit.*, pages 1717–1726, 2020. 3
- [44] Wenhan Yang, Robby T. Tan, Shiqi Wang, and Jiaying Liu. Self-learning video rain streak removal: When cyclic consistency meets temporal correspondence. In *Proc. IEEE/CVF Conf. Comput. Vis. Pattern Recognit.*, pages 1717–1726, 2020. 7
- [45] Hong You, Xian Zhong, Wenxuan Liu, Qi Wei, Wenxin Huang, Zhaofei Yu, and Tiejun Huang. Converting artificial neural networks to ultralow-latency spiking neural networks for action recognition. *IEEE Trans. Cogn. Dev. Syst.*, 16(4): 1533–1545, 2024. 3
- [46] Zongsheng Yue, Jianwen Xie, Qian Zhao, and Deyu Meng. Semi-supervised video deraining with dynamical rain generator. In *Proc. IEEE/CVF Conf. Comput. Vis. Pattern Recognit.*, pages 642–652, 2021. 3
- [47] Zongsheng Yue, Jianwen Xie, Qian Zhao, and Deyu Meng. Semi-supervised video deraining with dynamical rain generator. In *Proc. IEEE/CVF Conf. Comput. Vis. Pattern Recognit.*, pages 642–652, 2021. 2, 7
- [48] Jiyuan Zhang, Shiyang Chen, Yajing Zheng, Zhaofei Yu, and Tiejun Huang. Spike-guided motion deblurring with unknown modal spatiotemporal alignment. In *Proc. IEEE/CVF Conf. Comput. Vis. Pattern Recognit.*, pages 25047–25057, 2024. 3
- [49] Kaihao Zhang, Dongxu Li, Wenhan Luo, Wenqi Ren, and Wei Liu. Enhanced spatio-temporal interaction learning for video deraining: Faster and better. *IEEE Trans. Pattern Anal. Mach. Intell.*, 45(1):1287–1293, 2023. 2, 6, 7
- [50] Jing Zhao, Ruiqin Xiong, Jiyu Xie, Boxin Shi, Zhaofei Yu, Wen Gao, and Tiejun Huang. Reconstructing clear image for high-speed motion scene with a retina-inspired spike camera. *IEEE Trans. Computational Imaging*, 8:12–27, 2022. 3
- [51] Junwei Zhao, Shiliang Zhang, Lei Ma, Zhaofei Yu, and Tiejun Huang. Spikingsim: A bio-inspired spiking simulator. In *Proc. IEEE Int. Symp. Circuits Syst.*, pages 3003–3007, 2022. 6
- [52] Rui Zhao, Ruiqin Xiong, Jing Zhao, Jian Zhang, Xiaopeng Fan, Zhaofei Yu, and Tiejun Huang. Boosting spike camera image reconstruction from a perspective of dealing with spike fluctuations. In *Proc. IEEE/CVF Conf. Comput. Vis. Pattern Recognit.*, pages 24955–24965, 2024. 2
- [53] Yajing Zheng, Zhaofei Yu, Song Wang, and TieJun Huang. Spike-based motion estimation for object tracking through bio-inspired unsupervised learning. *IEEE Trans. Image Process.*, 32:335–349, 2023. 3
- [54] Xian Zhong, Tianyou Lu, Wenxin Huang, Mang Ye, Xuemei Jia, and Chia-Wen Lin. Grayscale enhancement colorization network for visible-infrared person re-identification. *IEEE Trans. Circuits Syst. Video Technol.*, 32(3):1418–1430, 2022. 1

- [55] Xian Zhong, Shengwang Hu, Wenxuan Liu, Wenxin Huang, Jianhao Ding, Zhaofei Yu, and Tiejun Huang. Towards low-latency event-based visual recognition with hybrid step-wise distillation spiking neural networks. In *Proc. ACM Int. Conf. Multimedia*, pages 9828–9836, 2024. [3](#)
- [56] Lin Zhu, Siwei Dong, Tiejun Huang, and Yonghong Tian. A retina-inspired sampling method for visual texture reconstruction. In *Proc. IEEE Int. Conf. Multimedia Expo*, pages 1432–1437, 2019. [7](#)
- [57] Lin Zhu, Siwei Dong, Jianing Li, Tiejun Huang, and Yonghong Tian. Ultra-high temporal resolution visual reconstruction from a fovea-like spike camera via spiking neuron model. *IEEE Trans. Pattern Anal. Mach. Intell.*, 45(1): 1233–1249, 2023. [2](#)
- [58] Lin Zhu, Siwei Dong, Jianing Li, Tiejun Huang, and Yonghong Tian. Ultra-high temporal resolution visual reconstruction from a fovea-like spike camera via spiking neuron model. *IEEE Trans. Pattern Anal. Mach. Intell.*, 45(1): 1233–1249, 2023. [2](#), [3](#)
- [59] Yaoyu Zhu, Yu Zhang, Xiaodong Xie, and TieJun Huang. An FPGA accelerator for high-speed moving objects detection and tracking with a spike camera. *Neural Comput.*, 34(8): 1812–1839, 2022. [3](#)

SpikeDerain: Unveiling Clear Videos from Rainy Sequences Using Color Spike Streams

Supplementary Material

1. Detail of Rain100C

1.1. Motivation of Rain100C

The motivation for building this dataset stems from some challenges in image processing tasks in current rainfall scenarios. In existing public datasets, the synthesis of raindrops or rain streaks often lacks sufficient realism, especially in depicting the continuity of raindrops and natural motion patterns. Due to simplification or excessive discretization in the generation process of rain streaks in many existing datasets, the synthesized images exhibit obvious local fractures, disjointed tails, or raindrop motion patterns that do not conform to physical laws. These inherent defects often become factors that affect the performance of algorithms in practical applications.

In Fig. 1, the top row shows the rain patterns synthesized from the existing public dataset, and the bottom row shows the rain patterns generated by this method. It can be observed that in existing datasets, there are often phenomena such as discontinuous rain patterns and abrupt tails (as shown in the red rectangular box), which make it difficult to reflect the coherent motion of real raindrops visually; The rain patterns generated by this method significantly improve these discontinuities, with smoother raindrop tails and more consistent physical laws in spatial distribution and brightness attenuation. This feature helps to provide more realistic and diverse training samples for image rain removal, object detection, and other computer vision tasks in rainy scenes, thereby improving the robustness and generalization ability of the algorithm in practical application scenarios.

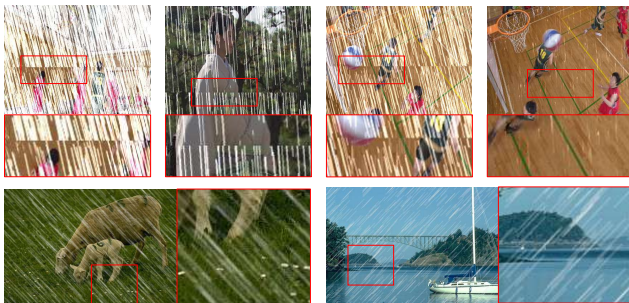


Figure 1. **Visual comparison between existing datasets and our method for generating rain streaks.** There is a phenomenon of discontinuous rain streaks in the existing dataset, while the rain streaks generated by this method are visually more natural and continuous.

1.2. Method of Construction

We propose a method that synthesizes continuous rain streaks by leveraging the underlying physics of rainfall. Our approach is summarized in the following theoretical formulation:

Firstly, an initial noise map $N(x, y)$ is generated via uniform random sampling. This noise is then processed using a threshold function to obtain:

$$N'(x, y) = \begin{cases} N(x, y), & \text{if } N(x, y) \geq 255 - v, \\ 0, & \text{otherwise,} \end{cases} \quad (1)$$

where v is a parameter controlling the noise level. This step ensures that only high-intensity noise is preserved, thereby better reflecting the local highlights of raindrops in the imaging process.

Subsequently, we construct a motion blur kernel $K(x, y)$ to simulate the trailing effect observed when raindrops are in high-speed motion. This kernel is designed based on the physical parameters of raindrops, such as the length L , width w , and tilt angle θ . The kernel construction can be conceptualized as initially forming a vertical line at the center of the kernel and then applying a rotation:

$$K'(x, y) = \text{rotate}(L(x, y), \theta), \quad (2)$$

with normalization such that:

$$\sum_{x, y} K'(x, y) = 1, \quad (3)$$

ensuring that the overall brightness of the image remains unchanged after convolution.

By convolving the processed noise map with the motion blur kernel, we obtain the rain streak map $R(x, y)$:

$$R(x, y) = (K * N')(x, y). \quad (4)$$

A linear fusion model is employed to synthesize the rainy image. The original image $I(x, y)$ is overlaid with the rain streak map $R(x, y)$ using a weighting coefficient β :

$$I_{\text{rain}}(x, y) = I(x, y) + \beta R(x, y), \quad (5)$$

where β controls the opacity of the rain streaks, ensuring that the original image details are retained while a natural rainy effect is achieved.

Furthermore, to capture the continuous motion of raindrops, spatial displacement parameters (h, w) are introduced.

For consecutive frames t , the rain streak map is smoothly translated, which is expressed as:

$$I_{\text{rain}}^{(t)}(x, y) = I(x, y) + \beta R(x - h_t, y - w_t). \quad (6)$$

This continuous spatial translation ensures temporal coherence in the generated data, more accurately reflecting the dynamic characteristics of raindrops in natural rainfall scenarios.

2. Theoretical Energy Consumption of SNNs

In the ablation studies of this paper, we compared the performance of models with different time steps, including the energy consumption calculation of spike neural networks. In this work, we calculated the theoretical energy consumption of different models.

The energy advantage of spiking neural networks (SNNs) primarily stems from their event-driven computation. In SNNs, synaptic operations occur only when a neuron’s membrane potential exceeds a threshold and a spike is triggered. This greatly reduces the actual number of operations compared to traditional neural networks. The theoretical energy consumption of an SNN can be estimated by counting the total number of synaptic operations (SOPs) that occur over all time steps. This can be expressed as:

$$N_{\text{SOP}} = s \times T \times A, \quad (7)$$

where s is the average sparsity of neuron activations (*i.e.*, the proportion of neurons that actually fire), T is the total number of simulation time steps, and A is the number of additive operations in the corresponding artificial neural network (ANN).

Furthermore, the total energy consumption of the SNN is given by the sum of the energy consumed by these synaptic operations and the energy used for spike generation:

$$E_{\text{SNN}} = N_{\text{SOP}} \times E_{\text{SOP}} + N_{\text{sign}} \times E_{\text{sign}}, \quad (8)$$

where, E_{SOP} denotes the energy consumption per synaptic addition operation, and E_{sign} represents the energy consumed by a spike (Sign operation) triggered by an LIF neuron. N_{sign} is the total number of spikes triggered. In contrast, a typical floating-point operation (FLOP) in a conventional ANN requires approximately 12.5pJ of energy. By leveraging low-energy additions and the sparse firing mechanism, SNNs exhibit a significant advantage in overall energy consumption.

This model, which is based on the statistics of the actual number of operations and the energy cost of different operation types, facilitates the theoretical quantification of the low-energy characteristics of SNNs and provides strong theoretical support for their implementation in efficient, resource-constrained devices.

3. More Qualitative Results

We present more qualitative comparisons on various datasets, shown in Fig. 2 to Fig. 6. It can be observed that our proposed method outperforms other state-of-the-art methods, with the best effects of rain removal and detail restoration.

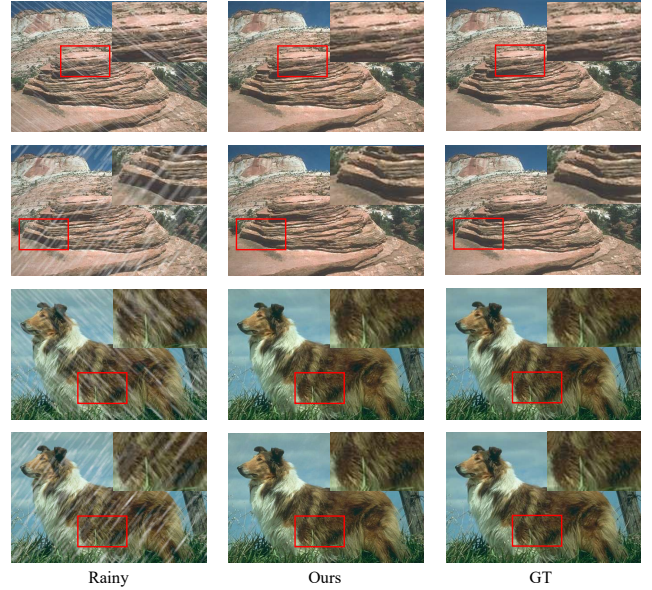


Figure 2. **Qualitative results on Rain100C.** Zoom-in for better visualization.

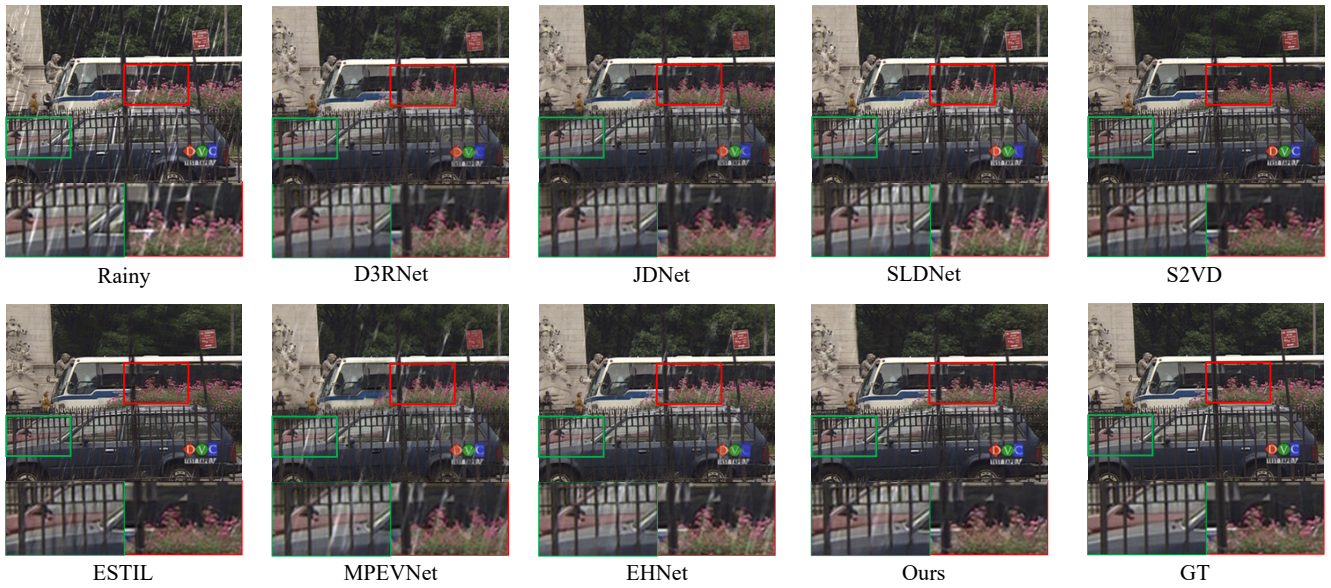


Figure 3. **Qualitative comparison on SynLight25.** Zoom-in for better visualization.

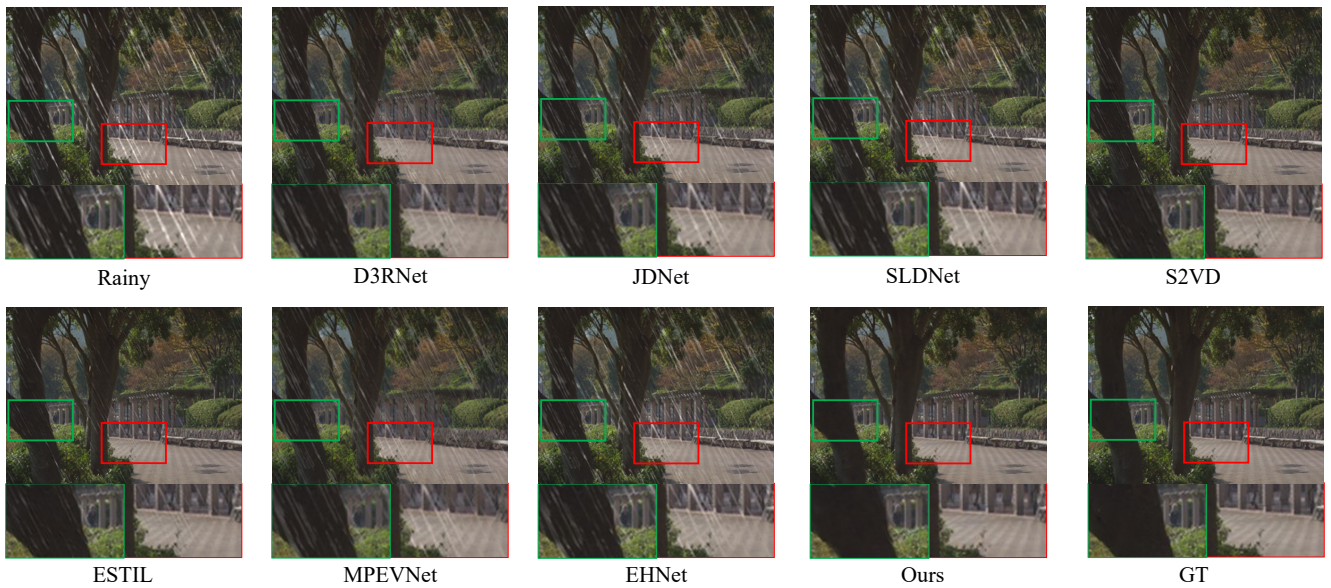


Figure 4. **Qualitative comparison on SynLight25.** Zoom-in for better visualization.

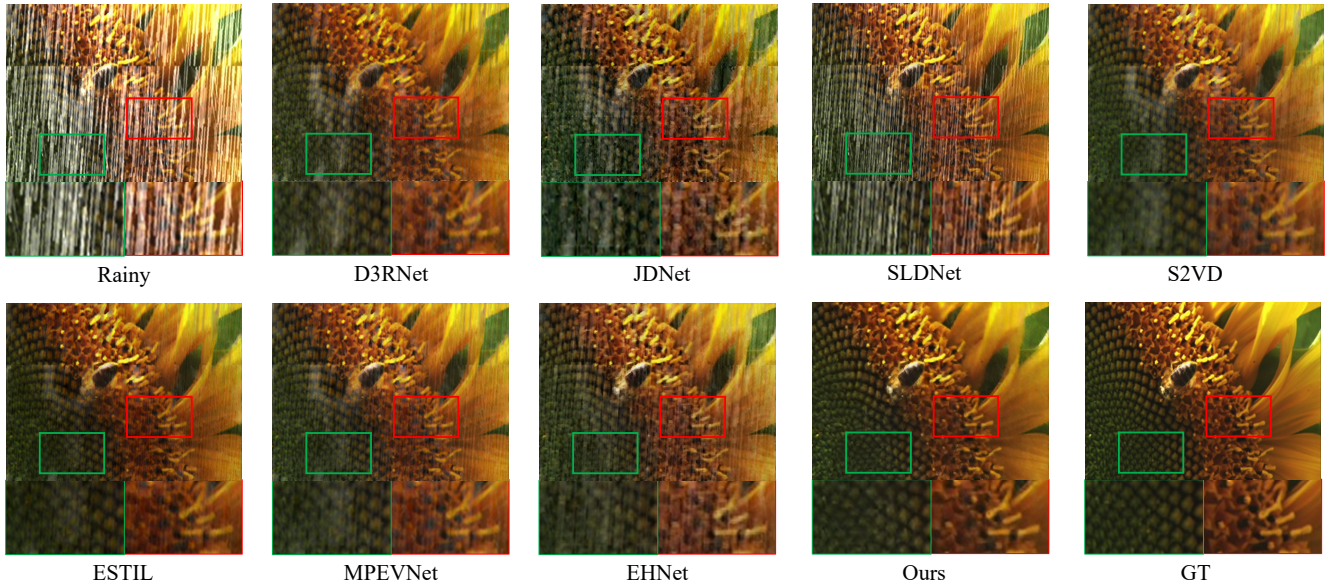


Figure 5. **Qualitative comparison on SynHeavy25.** Zoom-in for better visualization.



Figure 6. **Qualitative comparison on SynHeavy25.** Zoom-in for better visualization.